Enhanced release of ciliary extracellular vesicles suppresses cell migration and promotes cell aggregation

Tetsuhiro Hara[1,2,*], Ryota Nakazato[2,*], Kenji Shirakawa[1,2], Faryal Ijaz[2], Kenichiro Uemura[1], Shinya Takahashi[1], Koji Ikegami[2,‡]

[1] Department of Surgery, Graduate School of Biomedical and Health Sciences, Hiroshima University, 1-2-3 Kasumi, Minami-ku, Hiroshima 734-8553, Japan

[2] Department of Anatomy and Developmental Biology, Graduate School of Biomedical and Health Sciences, Hiroshima University, 1-2-3 Kasumi, Minami-ku, Hiroshima 734-8553, Japan

[*] These two authors equally contributed to this work.

[‡] The author for correspondence (k-ikegami@hiroshima-u.ac.jp)

Keywords

primary cilia, PDAC, extracellular vesicles, cell migration, cell aggregation

Running Title

Primary cilia-derived EVs promote cell mass formation

Abstract

A primary cilium is a hair-like organelle that protrudes from the cell surface in many cell types. Growing evidence indicates that extracellular vesicles are released from primary cilia, and research is increasingly focused on defining the functions of these cilia-derived EVs. EVs are known to modulate the behavior of various cancer cells, and structural and functional abnormalities in primary cilia have been reported in multiple cancer types. We previously demonstrated that PANC-1 cells, a human pancreatic ductal adenocarcinoma cell line, acquire enhanced primary cilia formation after surviving solitary culture conditions, and that their cilia contribute to tumor-like cell mass formation. Here, we explored part of the underlying mechanism of this phenotype by investigating the contribution of EVs released from the primary cilia of PANC-1 cells. Clonal PANC-1 generated by limiting dilution exhibited enhanced ciliogenesis and distinct ciliary morphologies compared with parental cells. These clones also released higher levels of cilia-derived EVs, including an expanded population of freely floating EVs within the culture environment. Biochemical analyses further showed that this increase was selective for primary cilia-derived EVs rather than reflecting a global rise in total EV production. Functionally, EV fractions enriched in cilia-derived EVs suppressed parental PANC-1 cell migration, altered cell morphology, and promoted cell aggregation, mimicking key behavioral traits of solitary condition-surviving PANC-1 clones. Together, these findings identify enhanced release of primary cilia-derived EVs as a distinct feature of PANC-1 cells adapted to solitary growth and suggest their potential involvement in the malignant and metastatic behaviors of pancreatic cancer.

Introduction

A primary cilium is a microtubule-based sensory organelle that is formed on the surface of almost all vertebrate cell types and functions to sense mechanical and chemical stimuli (Garcia-Gonzalo and Reiter, 2012). The dynamics of primary cilia is crucial for the regulation of cellular homeostasis including cell cycle control (Plotnikova *et al.*, 2009). Proper ciliary function is essential for accurate cell and tissue differentiation, as well as for normal organ and organismal development (Corbit *et al.*, 2005; Nusse, 2003; Pazour and Witman, 2003; Singla and Reiter, 2006). A group of disorders collectively termed ciliopathies, which involve structural defects or dysfunction of primary cilia, affect the architecture and function of multiple organs (Badano *et al.*, 2006).

Recent studies have demonstrated that the tips of primary cilia in cultured mammalian cells can be severed and released into the extracellular space as extracellular vesicles (Nager *et al.*, 2017; Phua *et al.*, 2017; Wang *et al.*, 2019). Although primary cilia have long been recognized as sensors of extracellular stimuli, such as hormones, growth factors, and fluid flow (Anvarian *et al.*, 2019), the physiological roles of primary cilia-derived vesicles in mammalian cells remain largely unclear (Ikegami and Ijaz, 2021). In contrast, similar EVs released from cilia or flagella of model organisms such as *Chlamydomonus* and *C. elegans* have been extensively characterized (Wang *et al.*, 2014; Wang *et al.*, 2024; Wood *et al.*, 2013). Notably, one study has reported that a type of glioma cell exhibits enhanced proliferative potential when cultured in medium enriched with primary cilia-derived EVs (Hoang-Minh *et al.*, 2018), suggesting that such vesicles may mediate intercellular communication and could be associated with the poor prognosis observed in ciliated tumor cells.

Primary cilia have also been implicated in carcinogenesis. In many cancer types, including pancreatic ductal adenocarcinoma (Chao *et al.*, 2022), primary cilia are frequently lost (Schimmack *et al.*, 2016). This loss is thought to occur during the early stages of oncogenic transformation and tumorigenesis (Menzl *et al.*, 2014; Seeley *et al.*, 2009). Inhibition of ciliogenesis has been reported to promote the malignant transformation of normal pancreatic ductal epithelial cells (Deng *et al.*, 2018; Kobayashi *et al.*, 2020). The loss of primary cilia is therefore considered to be strongly correlated with cancer progression (Hassounah *et al.*, 2012; Paul *et al.*, 2022; Seeger-Nukpezah *et al.*, 2013). However, a clinical study of PDAC patients reported that the presence of primary cilia is associated with an increased rate of lymph node metastasis and serves as an independent poor prognostic factor (Emoto *et al.*, 2014). Interestingly, similar context-dependent and even contradictory roles of

primary cilia have been reported in other cancer types as well (Han *et al.*, 2009; Wang *et al.*, 2021). In recent years, an increasing number of studies have suggested a relationship between primary cilia and resistance to chemotherapy (Chao *et al.*, 2022; Jenks *et al.*, 2018; Khan *et al.*, 2018; Kim *et al.*, 2022; Lee, 2023).

PANC-1 is a cell line originally established from a primary PDAC tumor (Lieber *et al.*, 1975). We previously reported that the ability to form primary cilia is enhanced in PANC-1 cells cultured under solitary conditions. Furthermore, we demonstrated that primary cilia promote the formation of tumor-like cell clusters in PANC-1 cells (Shirakawa *et al.*, 2025). In this study, we explored the underlying mechanisms by which primary cilia promote cell cluster formation in PANC-1 cells cultured under the solitary condition. We found that solitary-cultured PANC-1 cells not only exhibit increased ciliogenesis but also release larger amounts of primary cilia-derived EVs. Moreover, we demonstrated that these EVs suppress PANC-1 cell migration while altering cell morphology and promoting the formation of cell aggregates.

Materials and methods

Cell culture

A human pancreatic cancer cell line, PANC-1, was obtained from the RIKEN Bioresources Cell Bank (Ibaraki, Japan). Cells were maintained in RPMI-1640 (Wako) supplemented with 10% fetal bovine serum (FBS; Gibco) and cultured at 37 ºC in a humidified incubator with 5% CO_2. For routine passaging, cells were seeded onto 100-mm culture dishes and harvested using 0.25% trypsin-EDTA. Cell numbers were determined with a hemocytometer. Phase-contrast images of cultured cells were acquired using an inverted microscope (AE3000, SHIMADZU RIKA).

Antibodies

The following primary antibodies were used for immunofluorescence (IF) and/or western blotting (WB): ARL13B (rabbit polyclonal, 1:1,000 for IF and WB; 17711-1-AP, Proteintech), ARL13B (mouse monoclonal, 1:50 for IF; 66739-1-Ig, Proteintech), FOP (mouse monoclonal, 1:10,000 for IF; H00011116-M01, Abnova), ALIX (rabbit polyclonal, 1:1500 for WB; 12422-1-AP, Proteintech), GAPDH (mouse monoclonal, 1:3,000 for WB; MAB374, Millipore), KIF3A (rabbit polyclonal, 1:1000 for WB; 13930-1-AP, Proteintech),

IFT88 (rabbit polyclonal, 1:1,500 for WB; 13967-1-AP, Proteintech). Secondary antibodies include Alexa Fluor-conjugated antibodies for IF (1:1,000; Thermo Fisher Scientific) and horseradish peroxidase-conjugated antibodies for WB (1:10,000; Jackson Immuno Research Laboratories). To minimize appearance of false particles, all primary and secondary antibodies used for EVs detection were centrifuged at 20,000 × g for 30 min prior to use to remove protein or fluorophore aggregates.

Immunofluorescence staining

Cells grown on coverslips (MATSUNAMI) were fixed with 4% paraformaldehyde (PFA, pH 7.5) for 20 min at room temperature. Following fixation, cells were blocked and permeabilized with PBS containing 5% normal goat serum and 0.1% Triton X-100 for 1 h at room temperature. Cells were then incubated overnight at 4 ºC with primary antibodies diluted in the same blocking buffer. After washing with PBS, cells were incubated with Alexa Fluor-conjugated secondary antibodies and DAPI (1 μg/ml; DOJINDO) for 1 h at room temperature. Samples were mounted on glass slides using VECTASHIELD mounting medium (Vector Laboratories, Burlingame, CA). Fluorescence images were acquired using an epifluorescence microscope (DMI3000B, Leica) equipped with 100× objective lens, N.A. 1.40 or a laser scanning confocal microscope (STELLARIS 5, Leica) equipped with 63× objective lens, N.A. 1.40. Quantitative image analysis was performed using ImageJ software (National Institutes of Health, Bethesda, MD, USA).

Ciliary vesicle collection

FBS used for EVs collection was pre-depleted by ultracentrifugation at 100,000 × g to remove FBS-derived small EVs such as exosomes and ectosomes. After PANC-1 cells reached confluency, the culture medium was replaced with medium containing 1% pre-cleared FBS. Conditioned culture medium was collected 20-24 h later. EVs released into the culture medium were collected using a three-step differential centrifugation protocol. First, culture medium was centrifuged at 2,000 × g for 20 min to remove dead cells. The resulting supernatant was centrifuged at 10,000 × g for 30 min, followed by ultracentrifugation of the final supernatant at 100,000 × g for 3 h 10 min using an MLA-55 angle rotor (Beckman). Pellets were rinsed once with PBS and subsequently used for western blotting. For collecting EVs used in wound-healing assay and Actin staining, ultracentrifugation was performed using MLS-50 swing rotor (Beckman) with a glycerol cushion put at the bottom of the tubes to prevent deformation and rupture of EVs. Following ultracentrifugation, supernatant was

carefully removed, and the EV pellets were resuspended in RPMI-1640 medium containing 1% pre-cleared FBS for use in each experiment.

Western blotting analysis

Cells and EV pellets were lysed with 1× sodium dodecyl sulfate-polyacrylamide gel electrophoresis (SDS–PAGE) sample buffer (Wako) and heated at 95 ºC for 5 min. Samples were loaded onto an acrylamide gel to keep the ratio of EV to cell lysate identical for all proteins examined. Proteins separated in SDS-PAGE were then transferred onto polyvinylidene difluoride (PVDF) membranes (Merk Millipore, Burlington, MA, USA). Membranes were blocked with 5% bovine serum albumin (BSA) prepared in Tris-buffered saline containing 0.1% Tween-20 (TBST) at room temperature for 1 h, followed by incubation with primary antibodies diluted with 1% BSA/TBST at 4 ºC overnight. Following washes with TBST, membranes were incubated with horseradish peroxidase-conjugated secondary antibodies at room temperature for 1 h. Protein bands were visualized using ECL prime (GE Healthcare, Chicago, IL, USA) and detected with VersaDoc imaging system (Bio-Rad, Hercules, CA).

Knockdown with RNAi

The Dicer-substrate small interfering RNA (DsiRNA) duplexes used were previously reported (Shirakawa *et al.*, 2025). Clonal PANC-1 cells (clone #70) were seeded into 35-mm or 100-mm culture dishes at a density of 56,000-57,000 cells/cm^2. Cells were transfected with 1 nM DsiRNA and 2 nM DsiRNA on day 1 and day 3 using Lipofectamine RNAiMAX (Invitrogen) with the manufacturer's instruction. On day 5, the culture medium was replaced with medium containing 1% pre-cleared FBS. On day 6, cells were either fixed or solubilized for subsequent immunofluorescence or western blotting analysis. The conditioned medium was collected to precipitate EVs for western blotting.

Wound healing assay

Confluent parental PANC-1 cells were scratched using a sterile 200 µl plastic pipette tip, and the culture medium was immediately replaced with medium containing EVs collected from conditioned media of either parental or clonal PANC-1 cells. Images of the wound area were captured at 0 and 48 h post-scratch using a phase-contrast microscope. Wound closure was quantitated using ImageJ software.

Actin staining

Parental PANC-1 cells were treated with culture medium containing EVs collected from condition media of either parental or clonal PANC-1 cells. After 48 h of treatment, cells were fixed with 4% PFA. The cells were then incubated for 2 h at room temperature with PBS containing AlexaFluor 488-conjugated phalloidin (1:1,000; A12379, Invitrogen) and DAPI (1:1,000) to stain F-actin and nuclei, respectively. Fluorescence images were acquired using STELLARIS 5 confocal microscope. For quantification, five random fields per sample were captured, and the proportion of round-shaped cells was calculated relative to the total number of DAPI-stained cells.

Quantification

Quantitative analyses of microscopy images were performed using ImageJ software. Cells bearing primary cilia were determined by counting DAPI-stained nuclei co-localized with ARL13B-positive cilia. Primary cilia-derived EVs were quantified by counting ARL13B-positive, FOP-negative particles. Images were acquired using either an epifluorescence microscope (DMI3000B, Leica) or a confocal microscope (FV1000, Olympus). EV localization on cells was analyzed using the “Orthogonal Views” tool ImageJ. Band intensities in western blotting were measured using the “Gels” tool in ImageJ. All experiments were independently performed at least three times to ensure reproducibility.

Statistical analysis

Date are presented as mean ± standard error of the mean (SEM). Statistical significance between two groups was assessed using a two-tailed unpaired Student’s *t*-test. For comparisons among multiple groups, one-way analysis of variance followed by appropriate post hoc tests were performed. Differences were considered statistically significant at p values of < 0.05. All statistical analyses were conducted using GraphPad Prism software (GraphPad Software, Inc., San Diego, CA, USA).

Results

Clonal PANC-1 cells derived from solitary culture exhibited enhanced ciliogenesis and distinct ciliary morphologies

We utilized two previously established PANC-1 clones (clone #70 and #76) (Fig. S1A), which were characterized in our prior study as exhibiting enhanced cell mass formation in a ciliogenesis-dependent manner (Shirakawa *et al.*, 2025). To investigate whether primary cilia-derived EVs contribute to this phenotype, we first optimized culture conditions to minimize interference from serum-derived factors. In our previous study, PANC-1 cells were cultured in medium containing 10% FBS (Shirakawa *et al.*, 2025). Here, we examined whether the clonal PANC-1 cells could maintain their enhanced ciliogenesis capacity under serum-deprived conditions. Cells were grown to confluency and then cultured for an additional 24 h in medium containing 1% EV-depleted FBS (pre-cleared by ultracentrifugation), after which most subsequent analyses were performed (Fig. S1B). Under this condition, both clone #70 and clone #76 displayed a significantly higher proportion of ciliated cells compared with parental PANC-1 cells: 42.0 ± 1.7% and 44.2 ± 3.9%, respectively, versus 29.3 ± 2.0% in the parental line (Fig. S1C, S1D). Based on these results, we adopted this low-serum (1% EV-depleted FBS) culture condition to induce ciliogensis in all following experiments. Primary cilia and their basal bodies were reliably visualized by staining for ARL13B and FOP, respectively (Fig. S1E).

High-magnification imaging revealed numerous ARL13B-positive particles in clone #70 (Fig. 1A, arrowheads). In addition, cilia with a bulged morphology at their tips were frequently observed (Fig. 1A, arrow in enlarged image), as well as branched cilia (Fig. 1A, arrow in enlarged image), suggesting that PANC-1 clones surviving solitary culture conditions acquire diverse ciliary structural characteristics associated with EV emission. We thus performed a detailed morphological analysis of primary cilia, categorizing them into five distinct types: (1) ‘**Normal’**, (2) ‘**Bulged’**, characterized by a swollen ciliary tip, (3) ‘**Emission’**, defined by the presence of particles in close proximity to the cilium, (4) ‘**Very short’**, consisting of markedly shortened cilia (including those oriented perpendicular to focal plane), and (5) ‘**Branched’**, featuring two cilia protruding from a single basal body (Fig. 1B). The ‘Normal’ type predominated in all cell lines; however, its proportion was slightly but significantly reduced in the clonal PNAC-1 cells (Parental: 86.0 ± 1.0% vs. clone #70: 70.4 ± 3.8%, p = 0.012; vs. clone #76: 72.2 ± 3.6%, p = 0.012)(Fig. 1C). In contrast, the ‘Bulged’ type accounted for more than 15% of cilia in clones #70 and #76, significantly higher than in parental PANC-1 cells (Parental: 6.8 ± 1.3% vs. clone #70: 15.7 ± 2.4%, p = 0.020; vs. clone #76: 16.1 ± 2.2, p = 0.020)(Fig. 1C). Although less abundant overall, the ‘Emission’ type was also significantly enriched in clones #70 and #76 (Parental: 1.3 ± 0.2% vs. clone #70: 3.4 ± 0.6%, p = 0.062; vs. clone #76: 4.0 ± 1.1%, p = 0.044)(Fig. 1C). The ‘Very short’ type was

slightly more frequently in the clonal lines (Parental: 5.2 ± 1.3% vs. clone #70: 10.0 ± 1.8%, $p = 0.098$; vs. clone #76: 7.4 ± 1.4, $p = 0.323$)(Fig. 1C). The 'Branched' type was extremely rare (<1%) in both parental and clonal PANC-1 cells (Fig. 1C).

To further characterize the 'Bulged' type, we performed double immunofluorescence staining for ARL13B and acetylated-α-tubulin (Ac-tub), a major component of the ciliary axoneme. Based on Ac-tub staining, 'Bulged'-type cilia were divided into three subtypes: **'Ac-tub-negative'** (absence of Ac-tub signal within the bulge), **'Ac-tub-positive'** (Ac-tub signal extending into the bulge), and **'Circle'** (forming a ring-like tip structure)(Fig. S2A). The 'Ac-tub-negative' subtype was the most prevalent, and this trend was found to be statistically significant (Fig. S2B).

Primary cilia-derived EVs, including a larger population of floating EVs, increase in clonal PANC-1 cells derived from solitary culture

Given that clonal PANC-1 cells exhibited more than twofold increase in primary cilia with bulged tips or ARL13B-positive particles compared with parental cells (Fig. 1C), we next quantified putative primary cilia-derived EVs in confocal fluorescence images. To exclude the possibility that that the ARL13B-positive particles represented nonspecific signals, we performed double immunofluorescence staining using two independent primary antibodies: a rabbit polyclonal antibody (17711-1-Ap) and a mouse monoclonal antibody (66739-1-Ig). All primary and secondary antibodies were centrifuged prior to use to eliminate aggregates and false-positive puncta. ARL13B-positive particles were consistently labeled by both antibodies, regardless of their distance from the primary cilium, confirming the specificity of the signals (Fig. 2A).

Since very short or truncated primary cilia can appear similar to ARL13B-positve puncta, we established a conservative criterion for EV identification. ARL13-positive particles located in close proximity to FOP, a marker of the basal body, were classified as short or truncated cilia and excluded from quantification (Fig. 2B). Under this definition, ARL13B-positive particles positioned away from FOP were counted as primary cilia-derived EVs in randomly selected fields of view. Quantitative analysis revealed that the number of primary cilia-derived EVs was significantly higher in both clone #70 and clone #76 compared with parental PANC-1 cells (Parental: 2.7 ± 0.5 vs. clone #70: 12.0 ± 1.1, $p < 0.001$; vs. clone #76: 9.5 ± 1.0, $p < 0.001$)(Fig. 2C). These results indicate that the primary cilia in solitary condition-surviving PANC-1 clones possess a markedly enhanced capacity for EV release.

To further characterize where primary cilia-derived EVs reside within the cell culture environment, we analyzed their spatial distribution confocal images. EVs were categorized into three groups: '**floating'**, '**close to cells'** (including above, beneath, or between cells), and '**close to glass'** (Fig. 2D, 2E). In clone #70, which exhibited the highest overall ARL13-positive EV number (Fig. 2C), the number of ARL13B-positive EVs classified as 'non-floating' (i.e. close to cells or close to glass) was significantly greater than the number of floating EVs (floating: 11.8 ± 2.5; non-floating: 45.8 ± 3.2; $p < 0.001$)(Fig. 2F). The proportion of floating EVs was also significantly higher in clone #70 than in parental PANC-1 cells (Parental: 2.5 ± 1.2; clone #70: 11.8 ± 2.5; $p = 0.016$)(Fig .2G). Clone #76 showed a trend toward more floating EVs than parental cells, although the difference did not reach statistical significance (7.0 ± 1.9, $p = 0.133$)(Fig. 2G). These findings suggest that PANC-1 cells that survived solitary culture conditions release a greater number of EVs capable of dispersing freely into the culture medium compared with parental PANC-1 cells.

Clonal PANC-1 cells derived from solitary culture selectively increase the release of primary cilia-derived EVs

Given that clonal PANC-1 cells exhibited an increased number of putative freely dispersing ARL13B-positive EVs, we hypothesized that ARL13B-positive EVs would be recovered more abundantly from clonal PANC-1 cultures than from parental cell cultures. To quantify primary cilia-derived EVs release, we collected EVs from conditioned media using ultracentrifugation. Parental and clonal PANC-1 cells were grown to confluency and then cultured for an additional 24 h in medium containing 1% pre-cleared FBS prior to media collection. After sequential centrifugation steps to remove dead cells and debris, EV-containing pellets were obtained by ultracentrifugation (Fig. 3A). Both the EV pellets and corresponding cell layers remaining after media removal were solubilized in SDS-PAGE sample buffer and analyzed by western blotting for ARL13B (a primary cilia marker), ALIX (an exosome marker), and GAPDH (a cytoplasmic protein)(Fig. 3B). The release level of each protein was evaluated by calculating the ratio of its abundance in the EV pellet to that in the corresponding cell lysate (Fig. 3C). GAPDH was barely detectable in the EV pellets, indicating minimal contamination from cytoplasmic proteins and confirming successful EV isolation. The ratios of GAPDH in EV pellets to cell lysates were similarly low (~0.04) across all groups (Parental: 0.037 ± 0.005 vs. clone #70: 0.044 ± 0.006, $p = 0.836$; vs. clone #76: 0.041 ± 0.010%, $p = 0.836$)(Fig. 3B, 3C). Notably, ARL13B levels in the EV pellets were

significantly higher in clones #70 and #76 than in parental PANC-1 cells (Parental: 0.55 ± 0.03 vs. clone #70: 1.19 ± 0.12, $p = 0.001$; vs. clone #76: 1.09 ± 0.08, $p = 0.002$)(Fig. 3B, 3C). In contrast, ALIX levels in EV pellets did not differ significantly among the three cell types (Parental: 1.49 ± 0.18 vs. clone #70: 1.59 ± 0.15, $p = 0.649$; vs. clone #76: 1.78 ± 0.11, $p = 0.353$)(Fig. 3B, 3C). Together, these results demonstrate that PANC-1 cells surviving solitary culture conditions selectively enhance the release of primary cilia-derived EVs, rather than increasing EV production globally.

EVs enriched in primary cilia-derived EVs suppress cell migration and promote cell aggregation

We next sought to determine how the increased abundance of primary cilia-derived EVs in clonal PANC-1 cells affects cellular behaviors. However, both knockdown and knockout approaches proved unsuitable for functional disruption of ciliogenesis in our system. In knockdown experiments (Fig. S3A-S3C), siRNA-mediated suppression of IFT88 or KIF3A expression unexpectedly did increase the amounts of GAPDH, ARL13B, and ALIX detected in EV pellets compared with siNC-treated controls (Fig. S3D). These results suggest that inhibiting ciliogenesis triggers unintended leakage of cytoplasmic components into the culture medium, complicating the interpretation of EV-related phenotypes. Furthermore, in CRISPR/Cas9-mediated knockout experiments, we were unable to isolate any viable clones deficient in either IFT88 or KIF3A, despite screening more than 50 clones for each gene. These repeated failures prevented us from performing gene disruption-based analyses of ARL13B-positive EVs.

Given these limitations, we instead compared the biological effects of EVs collected from clonal PANC-1 cell cultures (clones #70 and #76) with those from parental PANC-1 cell cultures (Fig. 4A). To assess the impact of EVs on cell migration, we performed wound-healing assays. Confluent parental PANC-1 monolayers were scratched, and the medium was replaced with medium in which EVs collected from either the parental or clonal PANC-1 cell cultures had been resuspended (Fig. 4A). The recovered area was measured 48 h after wounding (Fig. 4B). Parental PANC-1 cells treated with EVs derived from clonal PANC-1 cells exhibited significantly reduced wound closure compared with those treated with parental EVs (Parental EVs: 9.9 ± 1.0% vs. clone #70 EVs: 7.5 ± 0.8%, $p = 0.086$; vs. clone #76 EVs: 5.5 ± 0.9%, $p = 0.015$)(Fig. 4B, 4C). These results indicate that primary cilia-derived EVs suppress PANC-1 cell migration.

We next examined the effects of EVs on cell aggregation, given our previous observation that clones #70 and #76 exhibit enhanced cell mass formation (Shirakawa *et al.*, 2025). Parental PANC-1 cells were treated with EVs derived from parental or clonal PANC-1 cultures, and nuclei were visualized by DAPI staining 48 h after treatment. Notably, cells treated with clonal-cell EVs formed more compact aggregates than those treated with parental-cell EVs (Fig. 4D). To further characterize the morphology of aggregated cells, we stained F-actin using fluorophore-conjugated phalloidin (Fig. 4E). The proportion of rounded PANC-1 cells was significantly higher in cultures treated with clonal EVs compared with parental EVs (Parental EVs: 5.5 ± 1.2% vs. clone #70 EVs: 19.2 ± 1.0%, $p < 0.001$; vs. clone #76: 20.3 ± 1.3%, $p < 0.001$)(Fig. 4F). Together, these results demonstrate that primary cilia-derived EVs from clonal PANC-1 cells not only inhibit migration but also promote cell aggregation and induce rounded cell morphology, implicating them as functional mediators of cell behavioral changes associated with solitary condition-surviving PANC-1 clones.

Discussion

One of the most important findings of this study is that clonal PANC-1 cells, which were grown from a single cell and exhibited an enhanced capacity of primary cilia formation, showed increased release of primary cilia-derived EVs. In the clonal cell culture, we observed numerous ARL13B-positive particles by immunofluorescence microscopy (Fig. 1 and 2). Since the identification of ARL13B-positive puncta could be subject to alternative interpretations, we implemented three rigorous experimental procedures to validate our conclusion. First, to eliminate the possibility that immunoglobulin aggregates or nonspecific fluorescent particles from the primary and secondary antibodies contributed to the observed signals, we centrifuged all antibodies at 20,000 × g for 30 min prior to use. Second, we performed dual immunostaining with two independent anti-ARL13B antibodies, ensuring that only particles labeled by both antibodies were considered ARL13B-positive. Third, to exclude the possibility that extremely short primary cilia might be misidentified as ARL13B-positive EVs, we classified ARL13B-positive particles as EVs only when they were spatially separated from the centriole. Together, these carefully designed controls strongly support our interpretation that the ARL13B-positive particles observed in the immunostaining analyses present primary cilia-derived EVs.

A high frequency of primary cilia with bulged tips was also observed in clonal

PANC-1 cells (Fig. 1). Primary cilia-derived EVs have been reported to be released through the accumulation of vesicular contents at the ciliary tip followed by pinching off, a process that depends on actin polymerization (Phua *et al.*, 2017). Our date indicate that the increase in primary cilia-derived EVs in clonal PANC-1 cell culture cannot be attributed solely to the higher number of primary cilia; rather, the EV-release capacity of these cells also appears to be enhanced. Specifically, the number of ARL13B-positive particles increased by approximately threefold in clonal cells compared with parental cells (Fig 2C), a difference that corresponds well to the combined effect of the ~1.5-fold increase in ciliogensis (Fig. S1D) and the ~2-fold increase in buldged-tip frequency (Fig. 1C). We further demonstrated that most ciliary tip bulges in clonal PANC-1 cells lacked acetylated tubulin (Fig. S2). This observation is consistent with our previous findings and other reports showing that EVs derived from primary cilia do not contain acetylated tubulin, a major structural component of the ciliary axoneme (Nager *et al.*, 2017; Phua *et al.*, 2017). Taken together, these results strongly support the interpretation that the bulges observed at ciliary tips in clonal PANC-1 cells represent structures that are released as primary cilia-derived EVs. Interestingly, although rare, we observed acetylated tubulin forming a ring-like ('Circle') structure at the distal ends of some primary cilia in clonal PANC-1 cells (Fig. S2). Such an unusual morphology has not been previously reported and might reflect aberrant structural features associated with the cancer cell state. In addition, we identified primary cilia that were split into two branches ('Branched'; Fig. 1), consistent with a recent report describing multiple ciliary projections emerging from a single basal body in human pancreatic islet cells by electron microscopy (Polino *et al.*, 2023). These atypical morphological features, branched cilia and circular ciliary tips, might therefore represent structural characteristics that are specific to pancreas-derived cells.

A greater number of primary cilia-derived EVs were detected on or between cells in clonal PANC-1 cell cultures (Fig. 2F). This observation suggests that EVs released from clonal PANC-1 cells are relatively 'sticky' and readily adhere to the cell surface. The much larger increase in EV-associated ARL13B-positive particles observed by immunostaining (3-4-fold higher in clonal cells than in parental cells; Fig. 2), compared with the more modest ~2-fold increase in ARL13B levels measured in EVs pellets from clonal PANC-1 culture media (Fig. 3), further supports the interpretation that many primary cilia-derived EVs remain attached to the cell surface of clonal PANC-1 cells. An alternate explanation, however, is that clonal PANC-1 cells themselves possess increased surface adhesiveness. Notably, elevated adhesiveness of EVs or of the cell surface is a known feature of mesenchymal cell types. For

example, ARL13B-positive cilia-derived EVs from fibroblasts such as NIH/3T3 cells or mouse embryonic fibroblast -both exhibiting mesenchymal characteristics- frequently remain attached to the plasma membrane (Phua *et al.*, 2017). Our previous work identified mesenchyme-like traits in PANC-1 clones that have survived solitary culture conditions, suggesting that increased cellular adhesiveness might be an intrinsic property of these clones. The enhanced adhesion of primary cilia-derived EVs released from clonal PANC-1 might have implication for the early metastatic behavior of PDAC. Cell adhesion has been recognized as a critical determinant of tumor metastasis, including the adhesive properties of EV surfaces and associated adhesion molecules (Jerabkova-Roda *et al.*, 2022). These findings raise the possibility that the strong adherence of cilia-derived EVs contribute to the mechanisms underlying the remarkably early metastasis characteristics of PDAC, one of the malignancies with the poorest prognosis (Kuehn, 2020; Sung *et al.*, 2021).

We collected EVs released into the culture medium by ultracentrifugation and analyzed their components by western blotting. The results showed that the amount of ARL13B was significantly increased in the EV pellets derived from clonal PANC-1 cell cultures compared with those from parental PANC-1 cells (Fig. 3). These findings provide strong evidence that the release of primary cilia-derived EVs is elevated in clonal PANC-1 cells. In contrast, the amount of ALIX (apoptosis-linked gene 2-interacting protein X) present in EV pellets was unchanged between clonal and parental PANC-1 cultures (Fig. 3). ALIX is a component of the endosomal sorting complex required for transport (ESCRT) complex and is widely used as a marker for exosomes (Matsuo *et al.*, 2004; Dowlatshahi *et al.*, 2012). The absence of changes in ALIX levels therefore suggests that the increase observed in clonal PANC-1 cells is specific to primary cilia-derived EVs rather than a global increase in EV production. Further investigation will be required to elucidate the mechanism underlying this selective enhancement of cilia-derived EV release.

We were unable to apply knockdown approaches effectively in the present study, despite having previously succeeded in suppressing primary cilia formation in PANC-1 cells by siRNA-mediated knockdown of KIF3A or IFT88 (Shirakawa *et al.*, 2025). In clonal PANC-1 cells, knockdown of KIF3A or IFT88 did not reduce the release of primary cilia-derived EVs into the culture medium (Fig. S3). Instead, the amounts of ARL13B, ALIX, and GAPDH detected in the culture medium were all increased compared with control siRNA-treated cells. These results suggest that inhibiting ciliogenesis in clonal PANC-1 cells induce unexpected cellular responses that mask or counteract the intended suppression of cilia-derived EV release. The negative impact of disrupting key ciliogenic genes was even

more evident in our attempts at gene knockout. We were unable to obtain KIF3A- or IFT88-knockout PANC-1 cells using CRISPR/Cas9, despite repeated attempts. This difficulty is consistent with several previous reports in which targeted gene knockout in PANC-1 cells was also failed, even when using CRISPR/Cas9 systems (Lentsch *et al.*, 2019; Meng *et al.*, 2025; Ramaker *et al.*, 2021). Other groups have similarly relied on knockdown rather than knockout strategies when investigating primary cilia-related genes in PANC-1 cells (Kobayashi *et al.*, 2017; Mashima *et al.*, 2022). To our knowledge, no studies have successfully suppressed primary ciliogenesis in PANC-1 cells by knocking out cilia-related genes. These collective observations suggest that primary cilia-related genes are essential for PANC-1 cell viability and that complete loss of these genes likely causes severe cellular damage or lethality, thereby preventing the establishment of viable knockout clones.

Several previous studies have investigated the effects of EVs, including exosomes, on cell migration. Multiple reports indicate that EVs function as chemoattractants in cancer cells, thereby promoting cell migration (Sung *et al.*, 2015; Sung and Weaver, 2017). In contrast, other studies have demonstrated that EVs can inhibit cell migration (Wu *et al.*, 2017; Liu *et al.*, 2023). Notably, EVs released from irradiated pancreatic cancer cells have been reported to suppress the migration and invasion of pancreatic cancer cells (Nakaoka *et al.*, 2025). These findings suggest that the effect of EVs on cell migration might depend on their cellular origin or situation. In this study, we showed that EVs containing an increased proportion of primary cilia-derived EVs, collected from clonal PANC-1 cell culture media, suppress the migration of parental PANC-1 cells in a wound-healing assay (Fig. 4A and 4B). Since the wound-healing assay does not generate a concentration gradient of added EVs, the observed effects likely reflect changes in cell motility rather than chemotactic responses to primary cilia-derived EVs. EVs derived from clonal PANC-1 cells also promoted the formation of cell masses, and the actin cytoskeleton of the cells within these masses exhibited a circular morphology (Fig. 4D). EVs have previously been reported to influence actin polymerization in recipient cells (Kapustin *et al.*, 2025; McAtee *et al.*, 2025). Our findings therefore suggest that primary cilia-derived EVs released from clonal PANC-1 cells might modulate actin polymerization and consequently inhibit cell migration in recipient cells. We have reported that primary cilia in PANC-1 cells promote the formation of cell masses (Shirakawa *et al.*, 2025). The present study demonstrates that mass formation in PANC-1 cells induced by primary cilia is, at least in part, mediated by primary cilia-derived EVs. Although EV-mediated mass formation might involve enhanced cell proliferation, increased cell adhesion observed in Figure 2 is also likely to be a contributing factor.

In conclusion, we demonstrated that pancreatic cancer cells derived from solitary conditions exhibit an increased release of primary cilia-derived EVs, and that this increase suppresses the migratory capacity of pancreatic cancer cells while promoting the formation of cell mass. Primary cilia in glioma cells have also been reported to release EVs, and although indirect effects cannot be excluded, these EVs enhanced glioma cell proliferation (Hoang-Minh *et al.*, 2018). Despite such observations, very few studies have examined the functional roles of primary cilia-derived EVs, and none have explored their relevance in cancer biology with the exception of the glioma study. Our findings therefore represent one of the few reports elucidating the function and potential significance of primary cilia-derived EVs released from cancer cells. Further investigation will be required to clarify the mechanisms responsible for the increased production of cilia-derived EVs in PANC-1 cells surviving solitary conditions and to determine how these EVs regulate cell migration and cell mass formation.

Acknowledgements

A part of this work was conducted in the Natural Science Center for Basic Research and Development at Hiroshima University (NBARD-00002) under the support from the MEXT Project to promote public utilization of advanced research infrastructure (Program for supporting the construction of core facilities; Grant Number JPMXS0441300023).

Funding

This work was supported in part by Nozomi-H Foundation to K.I. and Kaken-hi Kiban-C (22K08776) to K.U. and K.I.

Conflict of Interest Statement

The authors declare no competing interests.

Author Contribution Statement

Conceptualization: TH, RN, KI

Funding acquisition: KI, KU

Investigation: TH, RN, KS, FI

Project administration: KU, ST, KI

Supervision: KI

Writing-original draft: TH, RN, KI

Writing-review & editing: all authors

References

Anvarian, Z., Mykytyn, K., Mukhopadhyay, S., Pedersen, L.B., and Christensen, S.T. 2019. Cellular signalling by primary cilia in development, organ function and disease. *Nat. Rev. Nephrol.*, **15**: 199-219.

Badano, J.L., Mitsuma, N., Beales, P.L., and Katsanis, N. 2006. The ciliopathies: an emerging class of human genetic disorders. *Ann. Rev. Genomics Hum. Genet.*, **7**: 125-148.

Chao, Y.Y., Huang, B.M., Peng, I.C., Lee, P.R., Lai, Y.S., Chiu, W.T., Lin, Y.S., Lin, S.C., Chang, J.H., Chen, P.S., Tsai, S.J., and Wang, C.Y. 2022. ATM- and ATR-induced primary ciliogenesis promotes cisplatin resistance in pancreatic ductal adenocarcinoma. *J. Cell. Physiol.*, **237**: 4487-4503.

Corbit, K.C., Aanstad, P., Singla, V., Norman, A.R., Stainier, D.Y., and Reiter, J.F. 2005. Vertebrate Smoothened functions at the primary cilium. *Nature*, **437**: 1018-1021.

Deng, Y.Z., Cai, Z., Shi, S., Jiang, H., Shang, Y.R., Ma, N., Wang, J.J., Guan, D.X., Chen, T.W., Rong, Y.F., Qian, Z.Y., Zhang, E.B., Feng, D., Zhou, Q.L., Du, Y.N., Liu, D.P., Huang, X.X., Liu, L.M., Chin, E., Li, D.S., Wang, X.F., Zhang, X.L., and Xie, D. 2018. Cilia loss sensitizes cells to transformation by activating the mevalonate pathway. *J. Exp. Med.*, **215**: 177-195.

Dowlatshahi, D.P., Sandrin, V., Vivona, S., Shaler, T.A., Kaiser, S.E., Melandri, F., Sundquist, W.I., and Kopito, R.R. 2012. ALIX is a Lys63-specific polyubiquitin binding protein that functions in retrovirus budding. *Dev. Cell*, **23**: 1247-1254.

Emoto, K., Masugi, Y., Yamazaki, K., Effendi, K., Tsujikawa, H., Tanabe, M., Kitagawa, Y., and Sakamoto, M. 2014. Presence of primary cilia in cancer cells correlates with prognosis of pancreatic ductal adenocarcinoma. *Human Pathol.*, **45**: 817-825.

Garcia-Gonzalo, F.R. and Reiter, J.F. 2012. Scoring a backstage pass: mechanisms of ciliogenesis and ciliary access. *J. Cell Biol.*, **197**: 697-709.

Han, Y.G., Kim, H.J., Dlugosz, A.A., Ellison, D.W., Gilbertson, R.J., and Alvarez-Buylla, A. 2009. Dual and opposing roles of primary cilia in medulloblastoma development. *Nat. Med.*, **15**: 1062-1065.

Hassounah, N.B., Bunch, T.A., and McDermott, K.M. 2012. Molecular pathways: the role of primary cilia in cancer progression and therapeutics with a focus on Hedgehog signaling. *Clin. Cancer Res.*, **18**: 2429-2435.

Hoang-Minh, L.B., Dutra-Clarke, M., Breunig, J.J., and Sarkisian, M.R. 2018. Glioma cell proliferation is enhanced in the presence of tumor-derived cilia vesicles. *Cilia*, **7**: 6.

Ikegami, K. and Ijaz, F. 2021. Current understandings of the relationship between extracellular vesicles and cilia. *J. Biochem.*, **169**: 139-145.

Jenks, A.D., Vyse, S., Wong, J.P., Kostaras, E., Keller, D., Burgoyne, T., Shoemark, A., Tsalikis, A., de la Roche, M., Michaelis, M., Cinatl, J., Jr., Huang, P.H., and Tanos, B.E. 2018. Primary Cilia Mediate Diverse Kinase Inhibitor Resistance Mechanisms in Cancer. *Cell Rep.*, **23**: 3042-3055.

Jerabkova-Roda, K., Dupas, A., Osmani, N., Hyenne, V., and Goetz, J.G. 2022. Circulating extracellular vesicles and tumor cells: sticky partners in metastasis. *Trends Cancer*, **8**: 799-805.

Kapustin, A.N., Tsakali, S.S., Whitehead, M., Chennell, G., Wu, M.Y., Molenaar, C., Kutikhin, A., Chen, Y., Ahmad, S., Bogdanov, L., Sinitsky, M., Rubina, K., Clayton,

A., Verweij, F.J., Pegtel, D.M., Zingaro, S., Lobov, A., Zainullina, B., Owen, D., Parsons, M., Cheney, R.E., Warren, D.T., Humphries, M.J., Iskratsch, T., Holt, M., and Shanahan, C.M. 2025. Matrix-associated extracellular vesicles modulate human smooth muscle cell adhesion and directionality by presenting collagen VI. *Elife*, **12**: RP90375.

Khan, N.A., Garg, A.D., Agostinis, P., and Swinnen, J.V. 2017. Drug-induced ciliogenesis in pancreatic cancer cells is facilitated by the secreted ATP-purinergic receptor signaling pathway. *Oncotarget*, **9**: 3507-3518.

Kim, S.O., Kim, B.Y., and Lee, K.H. 2022. Synergistic effect of anticancer drug resistance and Wnt3a on primary ciliogenesis in A549 cell-derived anticancer drug-resistant subcell lines. *Biochem. Biophys. Res. Commun.*, **635**: 1-11.

Kobayashi, T., Nakazono, K., Tokuda, M., Mashima, Y., Dynlacht, B.D., and Itoh, H. 2017. HDAC2 promotes loss of primary cilia in pancreatic ductal adenocarcinoma. *EMBO Rep.*, **18**: 334-343.

Kobayashi, T., Tanaka, K., Mashima, Y., Shoda, A., Tokuda, M., and Itoh, H. 2020. CEP164 Deficiency Causes Hyperproliferation of Pancreatic Cancer Cells. *Front. Cell Dev. Biol.*, **8**: 587691.

Kuehn, B.M. 2020. Looking to Long-term Survivors for Improved Pancreatic Cancer Treatment. *JAMA*, **324**: 2242-2244.

Lee, K.H. 2023. Primary cilia: a novel research approach to overcome anticancer drug resistance. *Front. Mol. Biosci.*, **10**: 1270639.

Lentsch, E., Li, L., Pfeffer, S., Ekici, A.B., Taher, L., Pilarsky, C., and Grützmann, R. 2019. CRISPR/Cas9-Mediated Knock-Out of Kras(G12D) Mutated Pancreatic Cancer Cell Lines. *Int. J. Mol. Sci.*, **20**: 5706.

Lieber, M., Mazzetta, J., Nelson-Rees, W., Kaplan, M., and Todaro, G. 1975. Establishment of a continuous tumor-cell line (panc-1) from a human carcinoma of the exocrine pancreas. *Int. J. Cancer*, **15**: 741-747.

Liu, Y., Wang, C.-Q., Zhu, Y.-K., Xu, J.-F., Yin, S.-Q., Hu, Q.-J., and Yang, R.-Q. 2023. Macrophage-secreted exosomes inhibit breast cancer cell migration via the miR-101-3p/DLG5 axis. *Asian Pac. J. Trop. Biomed.*, **13**: 532-538.

Mashima, Y., Nohira, H., Sugihara, H., Dynlacht, B.D., Kobayashi, T., and Itoh, H. 2022. KIF24 depletion induces clustering of supernumerary centrosomes in PDAC cells. *Life Sci. Alliance*, **5**: e202201470.

Matsuo, H., Chevallier, J., Mayran, N., Le Blanc, I., Ferguson, C., Fauré, J., Blanc, N.S., Matile, S., Dubochet, J., Sadoul, R., Parton, R.G., Vilbois, F., and Gruenberg, J. 2004. Role of LBPA and Alix in multivesicular liposome formation and endosome organization. *Science*, **303**: 531-534.

McAtee, C., Patel, M., Hoshino, D., Sung, B.H., von Lersner, A., Shi, M., Hong, N.H., Young, A., Krystofiak, E., Zijlstra, A., and Weaver, A.M. 2025. Secreted exosomes induce filopodia formation. *bioRxiv : the preprint server for biology*.

Meng, H., Nan, M., Li, Y., Ding, Y., Fang, X., Ma, W., and Zhang, M. 2025. PD-L1 knockout or ZG16 overexpression inhibits PDAC progression and modulates TAM polarization. *Front. Immunol.*, **16**: 1510179.

Menzl, I., Lebeau, L., Pandey, R., Hassounah, N.B., Li, F.W., Nagle, R., Weihs, K., and

McDermott, K.M. 2014. Loss of primary cilia occurs early in breast cancer development. *Cilia*, **3**: 7.

Nager, A.R., Goldstein, J.S., Herranz-Pérez, V., Portran, D., Ye, F., Garcia-Verdugo, J.M., and Nachury, M.V. 2017. An Actin Network Dispatches Ciliary GPCRs into Extracellular Vesicles to Modulate Signaling. *Cell*, **168**: 252-263.e14.

Nakaoka, A., Salah, M., Ruixian, Z., Nakahana, M., Shimizu, Y., Qin, Q., Zhang, Q., Mukumoto, N., Kobayashi, K., Ikegaki, Y., Akasaka, H., Inubushi, S., Koma, Y., Ishihara, T., Miyawaki, D., Sasayama, T., and Sasaki, R. 2025. Radiation suppresses liver metastases via exosome secretion in pancreatic cancer cells. *Sci. Rep.*, **15**: 23712.

Nusse, R. 2003. Wnts and Hedgehogs: lipid-modified proteins and similarities in signaling mechanisms at the cell surface. *Development*, **130**: 5297-5305.

Paul, C., Tang, R., Longobardi, C., Lattanzio, R., Eguether, T., Turali, H., Bremond, J., Maurizy, C., Gabola, M., Poupeau, S., Turtoi, A., Denicolai, E., Cufaro, M.C., Svrcek, M., Seksik, P., Castronovo, V., Delvenne, P., de Laurenzi, V., Da Costa, Q., Bertucci, F., Lemmers, B., Pieragostino, D., Mamessier, E., Janke, C., Pinet, V., and Hahne, M. 2022. Loss of primary cilia promotes inflammation and carcinogenesis. *EMBO Rep.*, **23**: e55687.

Pazour, G.J. and Witman, G.B. 2003. The vertebrate primary cilium is a sensory organelle. *Curr. Opin. Cell Biol.*, **15**: 105-110.

Phua, S.C., Chiba, S., Suzuki, M., Su, E., Roberson, E.C., Pusapati, G.V., Schurmans, S., Setou, M., Rohatgi, R., Reiter, J.F., Ikegami, K., and Inoue, T. 2017. Dynamic Remodeling of Membrane Composition Drives Cell Cycle through Primary Cilia Excision. *Cell*, **168**: 264-279.e15.

Plotnikova, O.V., Pugacheva, E.N., and Golemis, E.A. 2009. Primary cilia and the cell cycle. *Methods Cell Biol.*, **94**: 137-160.

Polino, A.J., Sviben, S., Melena, I., Piston, D.W., and Hughes, J.W. 2023. Scanning electron microscopy of human islet cilia. *Proc. Natl. Acad. Sci. U. S. A.*, **120**: e2302624120.

Ramaker, R.C., Hardigan, A.A., Gordon, E.R., Wright, C.A., Myers, R.M., and Cooper, S.J. 2021. Pooled CRISPR screening in pancreatic cancer cells implicates co-repressor complexes as a cause of multiple drug resistance via regulation of epithelial-to-mesenchymal transition. *BMC Cancer*, **21**: 632.

Schimmack, S., Kneller, S., Dadabaeva, N., Bergmann, F., Taylor, A., Hackert, T., Werner, J., and Strobel, O. 2016. Epithelial to Stromal Re-Distribution of Primary Cilia during Pancreatic Carcinogenesis. *PloS One*, **11**: e0164231.

Seeger-Nukpezah, T., Little, J.L., Serzhanova, V., and Golemis, E.A. 2013. Cilia and cilia-associated proteins in cancer. *Drug Discov. Today Dis. Mech.*, **10**: e135-142.

Seeley, E.S., Carrière, C., Goetze, T., Longnecker, D.S., and Korc, M. 2009. Pancreatic cancer and precursor pancreatic intraepithelial neoplasia lesions are devoid of primary cilia. *Cancer Res.*, **69**: 422-430.

Shirakawa, K., Nakazato, R., Hara, T., Uemura, K., Ijaz, F., Takahashi, S., and Ikegami, K. 2025. A type of pancreatic cancer cells form cell clusters from a solitary condition in a primary ciliogenesis-dependent manner. *Med. Mol. Morphol.*, **58**: 213-226.

Singla, V. and Reiter, J.F. 2006. The primary cilium as the cell's antenna: signaling at a

sensory organelle. *Science*, **313**: 629-633.

Sung, B.H., Ketova, T., Hoshino, D., Zijlstra, A., and Weaver, A.M. 2015. Directional cell movement through tissues is controlled by exosome secretion. *Nat. commun.*, **6**: 7164.

Sung, B.H. and Weaver, A.M. 2017. Exosome secretion promotes chemotaxis of cancer cells. *Cell adh. Migr.*, **11**: 187-195.

Sung, H., Ferlay, J., Siegel, R.L., Laversanne, M., Soerjomataram, I., Jemal, A., and Bray, F. 2021. Global Cancer Statistics 2020: GLOBOCAN Estimates of Incidence and Mortality Worldwide for 36 Cancers in 185 Countries. *CA Cancer J Clin.*, **71**: 209-249.

Wang, B., Liang, Z., and Liu, P. 2021. Functional aspects of primary cilium in signaling, assembly and microenvironment in cancer. *J. Cell. Physiol.*, **236**: 3207-3219.

Wang, G., Hu, H.B., Chang, Y., Huang, Y., Song, Z.Q., Zhou, S.B., Chen, L., Zhang, Y.C., Wu, M., Tu, H.Q., Yuan, J.F., Wang, N., Pan, X., Li, A.L., Zhou, T., Zhang, X.M., He, K., and Li, H.Y. 2019. Rab7 regulates primary cilia disassembly through cilia excision. *J. Cell Biol.*, **218**: 4030-4041.

Wang, J., Saul, J., Nikonorova, I.A., Cruz, C.N., Power, K.M., Nguyen, K.C., Hall, D.H., and Barr, M.M. 2024. Ciliary intrinsic mechanisms regulate dynamic ciliary extracellular vesicle release from sensory neurons. *Curr. Biol.*, **34**: 2756-2763.e2.

Wang, J., Silva, M., Haas, L.A., Morsci, N.S., Nguyen, K.C., Hall, D.H., and Barr, M.M. 2014. C. elegans ciliated sensory neurons release extracellular vesicles that function in animal communication. *Curr. Biol.*, **24**: 519-525.

Wood, C.R., Huang, K., Diener, D.R., and Rosenbaum, J.L. 2013. The cilium secretes bioactive ectosomes. *Curr. Biol.*, **23**: 906-911.

Wu, Q., Wu, X., Ying, X., Zhu, Q., Wang, X., Jiang, L., Chen, X., Wu, Y., and Wang, X. 2017. Suppression of endothelial cell migration by tumor associated macrophage-derived exosomes is reversed by epithelial ovarian cancer exosomal lncRNA. *Cancer Cell Int.*, **17**: 62.

Figure Legends

Figure 1. Enhanced EV-related structures and morphological diversity of primary cilia in clonal PANC-1 cells.

(A) Representative immunofluorescence images showing branched cilia (arrow), bulged ciliary tips (arrow), and vesicles (arrowheads) in clone #70 cells. Scale bar, 20 µm (main image) and 2 µm (enlarged views). **(B)** Representative immunofluorescence images showing classification of five primary cilium morphologies. Scale bars, 10 µm. **(C)** Quantification of each ciliary morphology. Data represent mean ± SEM from four independent experiments. Statistical significance was defined as $p < 0.05$, determined using one-way ANOVA.

Figure 2. Increased production and spatial dispersion of cilia-derived EVs by clonal PANC-1 cells.

(A) Immunostaining of vesicles and primary cilia using anti-ARL13B antibodies (red: 17711-1-AP; green: 66379-1-Ig). Scale bar, 5 µm. **(B)** Immunostaining for ARL13B (red) and FOP (green) to define EVs. EVs were defined as ARL13B-positive particles located away from FOP staining, whereas particles merged with or adjacent to FOP were classified as non-EVs. Scale bar, 5 µm. **(C)** Quantification of EV numbers in parental and clonal PANC-1 cells. Date represent mean ± SEM from 4 independent experiments. **(D)** Schematic illustration of the classification of EV locations. **(E)** Representative immunofluorescence images showing the five EV spatial categories. Upper: maximum-projection x-y images. Lower: x-z cross-sectional images taken at the yellow line in x-y images. Scale bar, 20 µm. **(F)** Quantification of 'floating EVs' and 'non-floating EVs' in clone #70. Data represent mean ± SEM from 4 independent experiments. **(G)** Quantification of floating EVs in parental and clonal PANC-1 cells. Data represent mean ± SEM from 4 independent experiments. Statistical significance was defined as $p < 0.05$ and assessed using one-way ANOVA (panels C and G) or two-tailed unpaired Student's *t*-test (panel F).

Figure 3. Selective enhancement of primary cilia-derived EV release in clonal PANC-1 cells.

(A) Schematic overview of the procedure used for EV collection. **(B)** Representative western blots showing ARL13B, ALIX, and GAPDH levels in cell lysates and in EV pellets obtained from the conditioned medium of parental and clonal PANC-1 cells. **(C)** Quantitative analyses of the pellet-to-cell lysate ratio for each protein (ARL13B, ALIX, and GAPDH). Data

represent mean ± SEM from four independent experiments. Statistical significance was defined as $p < 0.05$ and assessed using one-way ANOVA.

Figure 4. Suppression of cell migration and promotion of cell aggregation by clonal PANC-1 cell-derived EVs.

(A) Schematic overview of the experimental procedure for treating parental PANC-1 cells with primary cilia-derived EV-enriched EVs. **(B)** Representative phase-contrast images of wound closure in parental PANC-1 cells treated with EVs collected from parental or clonal PANC-1 cultures (and #76). Images were captured at 0 h and 48 h after wound creation. The initial wound edge (0 h) is indicated by white lines, and the boundary of the recovered area at 48 h is indicated by blue lines. Scale bars, 200 µm. **(C)** Quantification of recovered wound area at 48 h in parental PANC-1 cells treated with EVs from parental PANC-1 (blue) or clonal PANC-1 #70 or #76 (red), presented in pixels (pxl). **(D)** Fluorescence images of nuclei (DAPI) in parental PANC-1 cells treated with EVs from parental or clonal PANC-1 cultures (and #76) for 48 h. Arrows indicate aggregated cells. Scale bars, 200 µm. **(E)** Representative fluorescence images showing cell morphology in parental PANC-1 cells treated with EVs from parental or clonal PANC-1 cultures (and #76) for 48 h. Arrows indicate round-shaped cells. Scale bars, 50 µm. **(F)** Quantification of round-shaped cells in parental PANC-1 cultures treated with EVs from parental PANC-1 (blue) or clonal PANC-1 #70 or #76 (red) for 48 h. For panels (C) and (F), Statistical significance was defined as $p < 0.05$ was defined as and assessed using one-way ANOVA.

Figure S1. Validation of enhanced primary cilia formation in clonal PANC-1 cells under low-serum conditions.

(A) Representative phase-contrast images of parental and clonal PANC-1 cells (clone #70 and clone #76) acquired using an inverted microscope (DMI3000B, Leica) equipped with a 4× (top) and 10× (bottom) objective lenses. Scale bars, 200 µm. **(B)** Schematic overview of experimental conditions optimized to minimize nonspecific effects of serum-derived factors on experiments. **(C)** Representative immunofluorescence staining of nuclei (DAPI, upper) and primary cilia (ARL13B, lower) in parental and clonal PANC-1 cells. Scale bars, 20 µm. **(D)** Quantification of the proportion of ciliated cells shown in (C). Data represent mean ± SEM from three independent experiments. Statistical significance was defined as $p < 0.05$ and assessed using one-way ANOVA. **(E)** Immunofluorescence staining of nuclei (DAPI, blue), primary cilia (ARL13B, red), and centrioles marking the basal boy (FOP, green) in

parental and clonal PANC-1 cells. Scale bars, 50 µm.

Figure S2. Three morphological types of bulged ciliary tips.

(A) Representative immunofluorescence images showing three morphological types of bulged ciliary tips. Primary cilia are labeled with ARL13B (magenta), and ciliary axonemes with acetylated-α-tubulin (Ac-tub, green). Scale bars, 10 µm (main image) and 1 µm (insets). **(B)** Quantitative analysis of ciliary tip morphologies classified as shown in (A). Data represent mean ± SEM from five independent experiments. Statistical significance was defined as $p < 0.05$ and assessed using one-way ANOVA.

Figure S3. siRNA-mediated knockdown experiments.

(A) Immunostaining for primary cilia (red, ARL13B) and nuclei (blue, DAPI) was performed in clone #70 following treatment with siRNAs targeting negative control, IFT88, or KIF3A. Immunofluorescence staining confirmed a marked reduction in the number of ciliated cells after IFT88 or KIF3A knockdown compared with negative control (siNC). Scale bars, 50 µm. **(B)** Western blots showing ARL13B, IFT88, KIF3A, and GAPDH protein levels in clone #70 after treatment with NC, IFT88, or KIF3A siRNAs. Western blot analysis also demonstrated a significant decrease in IFT88 and KIF3A protein expression by IFT88 and KIF3A knockdown, respectively, relative to siNC. **(C)** Schematic diagram of the experimental procedure for siRNA knockdown and subsequent EV collection. **(D)** Western blots of ARL13B, ALIX, and GAPDH in cell lysates and EV pellets collected from clone #70 cultures following treatment with NC, IFT88, or KIF3A siRNAs. Unexpectedly, siRNA-mediated suppression of IFT88 or KIF3A expression increased the amounts of GAPDH, ARL13B, and ALIX in EV pellets compared with siNC-treated controls.

Figure 1

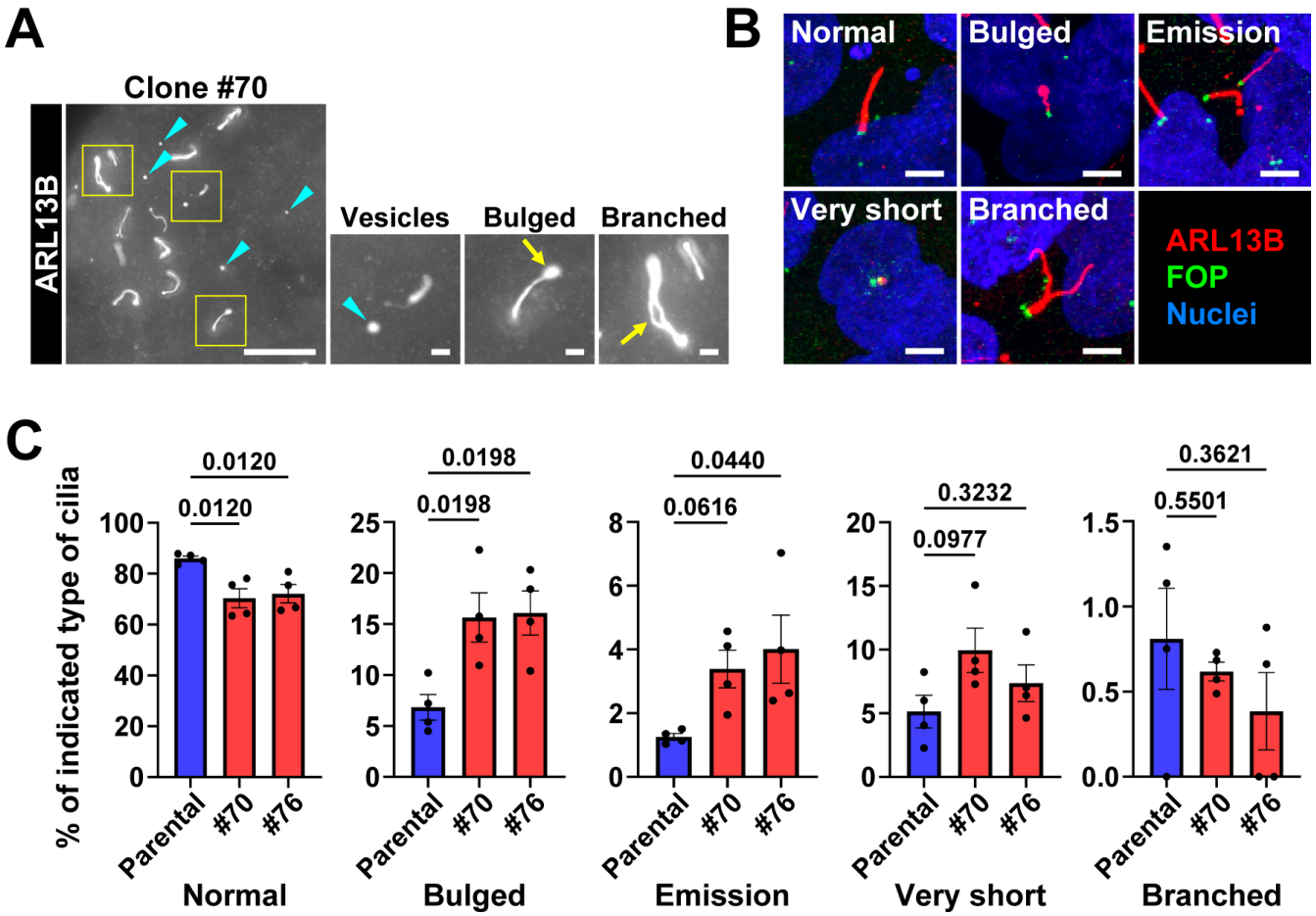
A
Clone #70
ARL13B
Vesicles
Bulged
Branched
B
Normal
Bulged
Emission
Very short
Branched
ARL13B
FOP
Nuclei
C
% of indicated type of cilia
0.0120
0.0120
0.0198
0.0198
0.0440
0.0616
0.3232
0.0977
0.3621
0.5501
Parental
#70
#76
Normal
Bulged
Emission
Very short
Branched

Figure 2

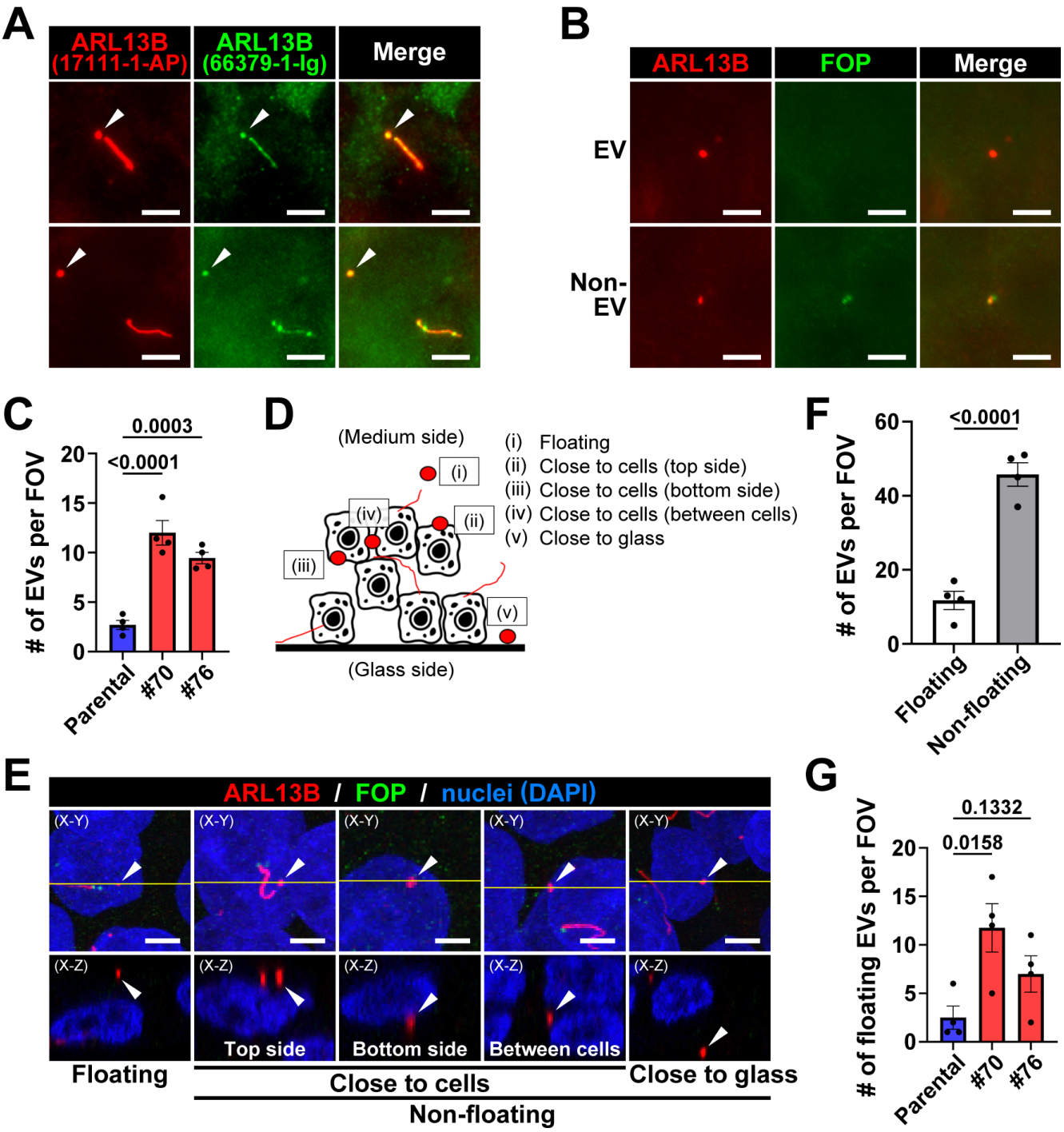
A
ARL13B (17111-1-AP)
ARL13B (66379-1-Ig)
Merge
B
ARL13B
FOP
Merge
EV
Non-EV
C
0.0003
<0.0001
# of EVs per FOV
20
15
10
5
0
Parental
#70
#76
D
(Medium side)
(i)
(ii)
(iii)
(iv)
(v)
(Glass side)
(i) Floating
(ii) Close to cells (top side)
(iii) Close to cells (bottom side)
(iv) Close to cells (between cells)
(v) Close to glass
F
<0.0001
# of EVs per FOV
60
40
20
0
Floating
Non-floating
E
ARL13B / FOP / nuclei (DAPI)
(X-Y)
(X-Z)
Top side
Bottom side
Between cells
Floating
Close to cells
Close to glass
Non-floating
G
0.1332
0.0158
# of floating EVs per FOV
20
15
10
5
0
Parental
#70
#76

Figure 3

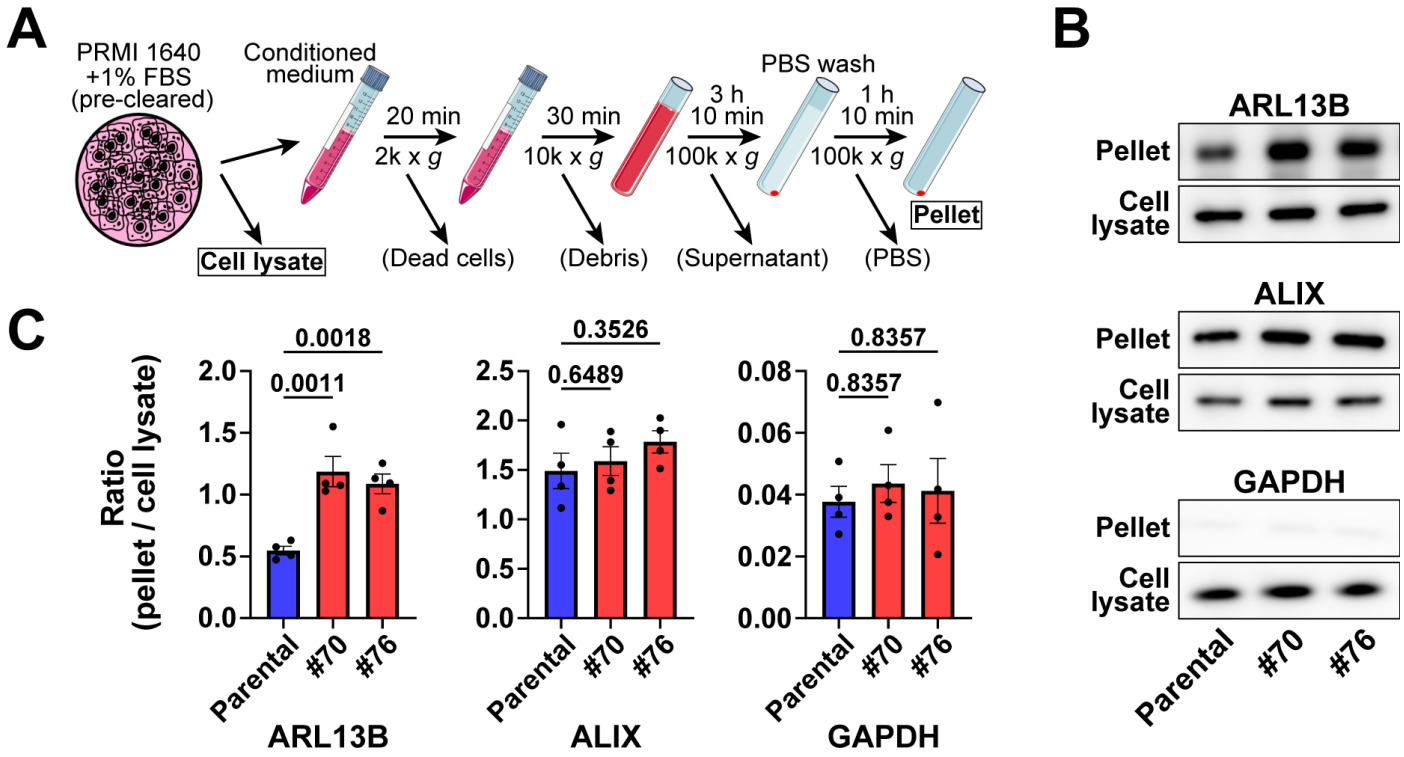
A
PRMI 1640
+1% FBS
(pre-cleared)
Conditioned
medium
Cell lysate
20 min
2k x g
(Dead cells)
30 min
10k x g
(Debris)
3 h
10 min
100k x g
(Supernatant)
PBS wash
1 h
10 min
100k x g
(PBS)
Pellet
B
ARL13B
Pellet
Cell
lysate
ALIX
Pellet
Cell
lysate
GAPDH
Pellet
Cell
lysate
Parental
#70
#76
C
Ratio
(pellet / cell lysate)
0.0018
0.0011
0.3526
0.6489
0.8357
0.8357
Parental
#70
#76
ARL13B
ALIX
GAPDH

Figure 4

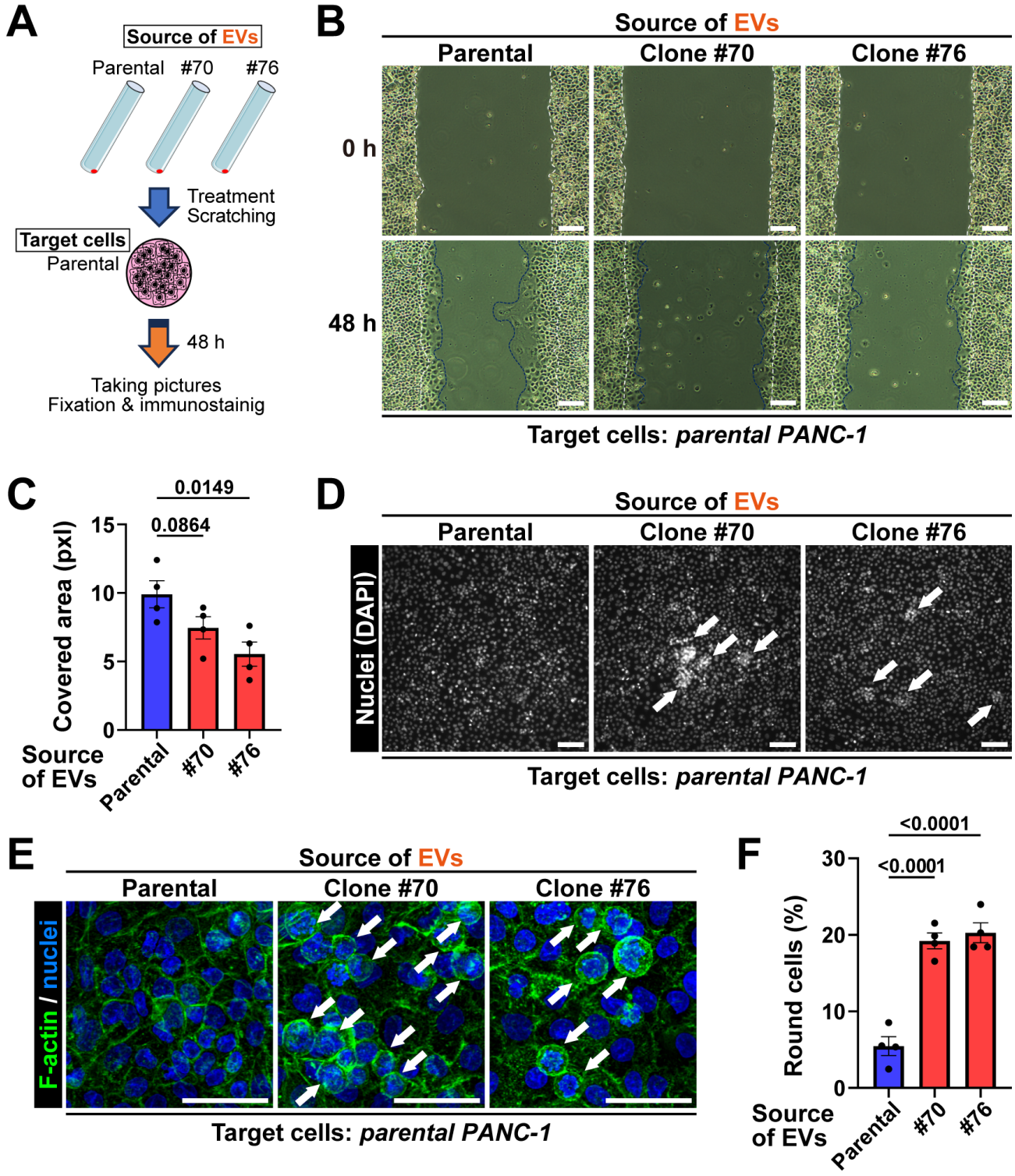
A
Source of EVs
Parental
#70
#76
Treatment
Scratching
Target cells
Parental
48 h
Taking pictures
Fixation & immunostainig
B
Source of EVs
Parental
Clone #70
Clone #76
0 h
48 h
Target cells: parental PANC-1
C
0.0149
0.0864
Covered area (pxl)
15
10
5
0
Source of EVs
Parental
#70
#76
D
Source of EVs
Parental
Clone #70
Clone #76
Nuclei (DAPI)
Target cells: parental PANC-1
E
Source of EVs
Parental
Clone #70
Clone #76
F-actin / nuclei
Target cells: parental PANC-1
F
<0.0001
<0.0001
Round cells (%)
30
20
10
0
Source of EVs
Parental
#70
#76

Figure S1

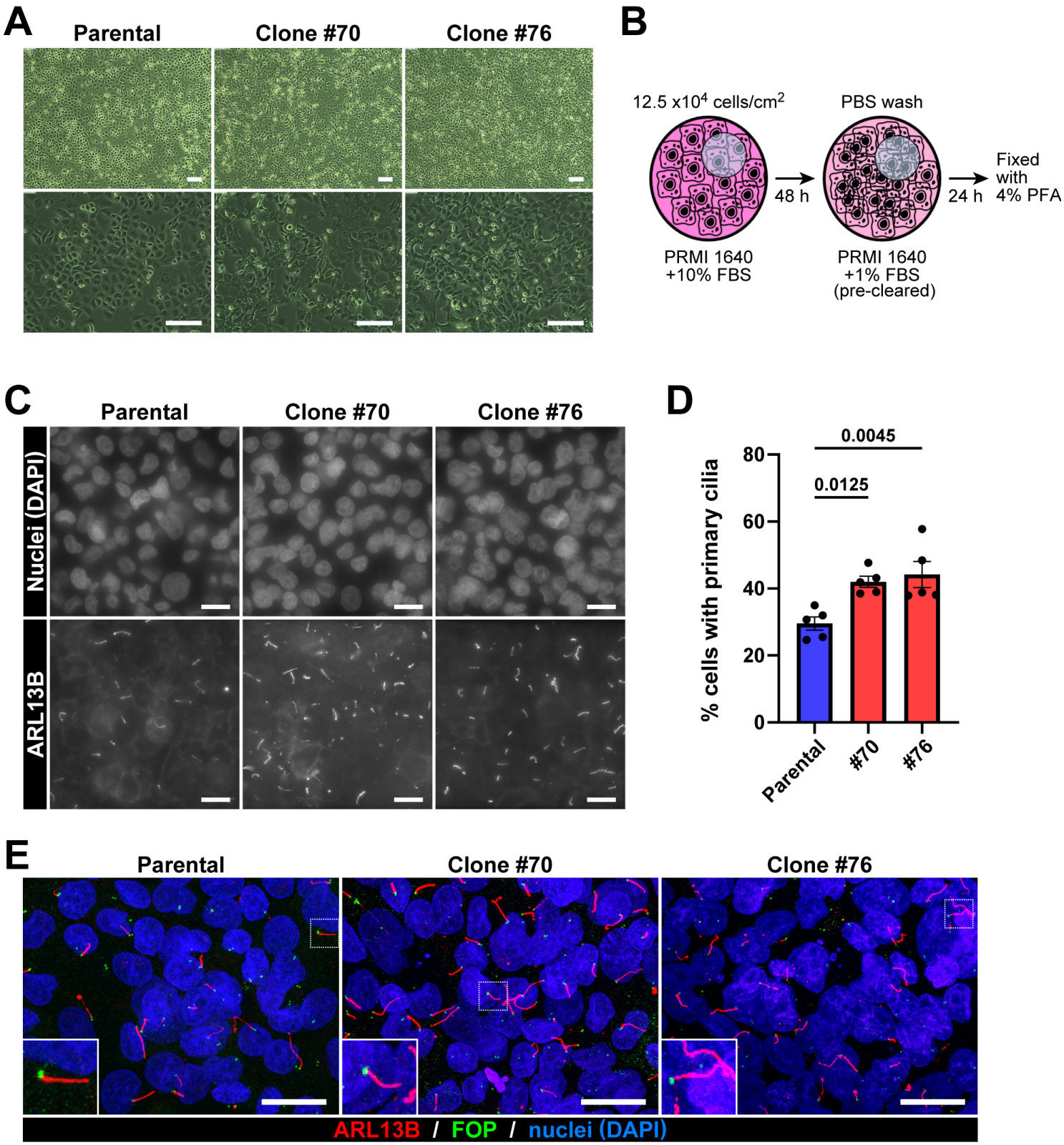
A
Parental
Clone #70
Clone #76
B
12.5 x10^4 cells/cm^2
PBS wash
48 h
24 h
Fixed with 4% PFA
PRMI 1640 +10% FBS
PRMI 1640 +1% FBS (pre-cleared)
C
Parental
Clone #70
Clone #76
Nuclei (DAPI)
ARL13B
D
% cells with primary cilia
0.0045
0.0125
80
60
40
20
0
Parental
#70
#76
E
Parental
Clone #70
Clone #76
ARL13B / FOP / nuclei (DAPI)

Figure S2

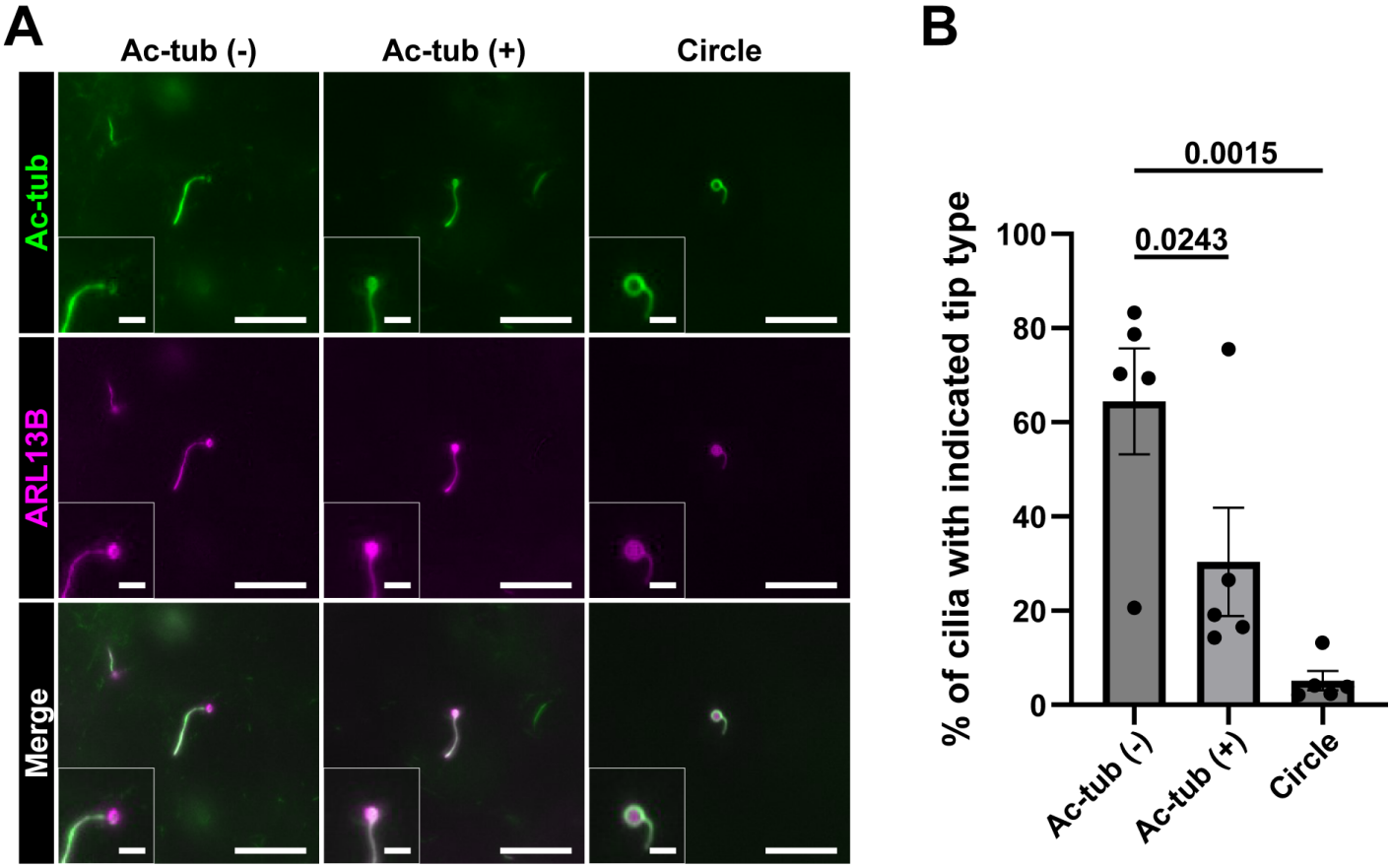
A
Ac-tub (-)
Ac-tub (+)
Circle
Ac-tub
ARL13B
Merge
B
0.0015
0.0243
% of cilia with indicated tip type
100
80
60
40
20
0
Ac-tub (-)
Ac-tub (+)
Circle

Figure S3

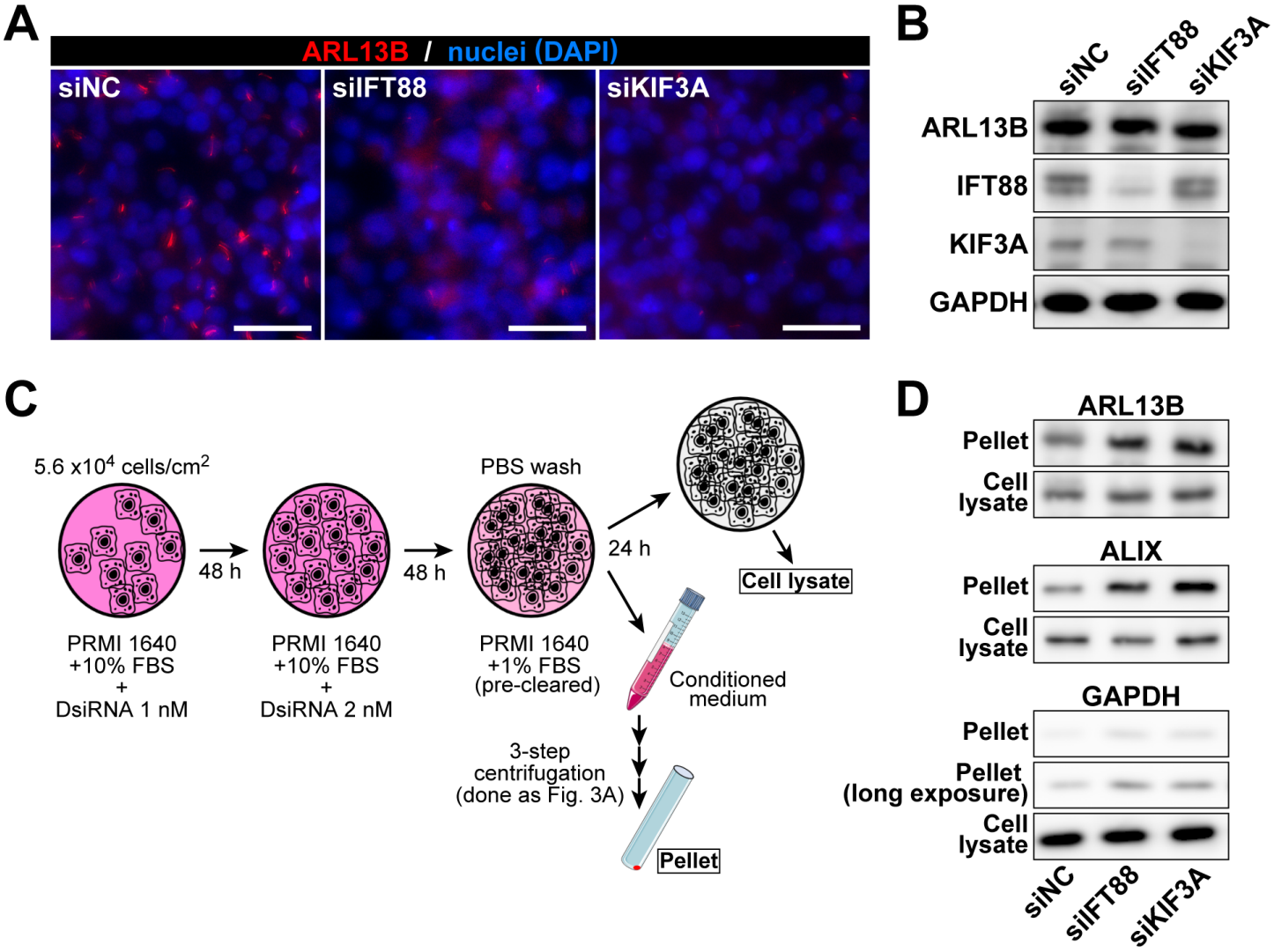
A
ARL13B / nuclei (DAPI)
siNC
siIFT88
siKIF3A
B
siNC
siIFT88
siKIF3A
ARL13B
IFT88
KIF3A
GAPDH
C
5.6 x10^4 cells/cm^2
48 h
48 h
PBS wash
24 h
PRMI 1640
+10% FBS
+
DsiRNA 1 nM
PRMI 1640
+10% FBS
+
DsiRNA 2 nM
PRMI 1640
+1% FBS
(pre-cleared)
Cell lysate
Conditioned medium
3-step centrifugation (done as Fig. 3A)
Pellet
D
ARL13B
Pellet
Cell lysate
ALIX
Pellet
Cell lysate
GAPDH
Pellet
Pellet (long exposure)
Cell lysate
siNC
siIFT88
siKIF3A